Quarterly Technical Report

Growth, Characterization and Device Development in Monocrystalline Diamond Films

Supported under Grant #N00014-93-I-0437
Office of the Chief of Naval Research
Report for the period 7/1/94–9/30/94

R. F. Davis, J. T. Glass, and R. J. Nemanich*
L. Bergman, M. McClure and K. Turner
North Carolina State University
c/o Materials Science and Engineering Department
*Department of Physics
Raleigh, NC 27695

September, 1994

REPORT DOCUMENTATION PAGE

Form Approved
OMB No. 0704-0188

1. AGENCY USE ONLY (Leave blank)	2. REPORT DATE	3. REPORT TYPE AND DATES COVERED
	September, 1994	Quarterly Technical 7/1/94–9/30/94

4. TITLE AND SUBTITLE

Growth, Characterization and Device Development in Monocrystalline Diamond Films

5. FUNDING NUMBERS

s400003srr14
1114SS
N00179
N66005
4B855

6. AUTHOR(S)

Robert F. Davis, J. T. Glass and R. J. Nemanich

7. PERFORMING ORGANIZATION NAME(S) AND ADDRESS(ES)

North Carolina State University
Hillsborough Street
Raleigh, NC 27695

8. PERFORMING ORGANIZATION REPORT NUMBER

N00014-93-1-0437

9. SPONSORING/MONITORING AGENCY NAMES(S) AND ADDRESS(ES)

Sponsoring: ONR, Code 1114, 800 N. Quincy, Arlington, VA 22217-5660
Monitoring: Office of Naval Research Resider
The Ohio State University Research Center
1960 Kenny Road
Columbus, OH 43210-1063

10. SPONSORING/MONITORING AGENCY REPORT NUMBER

11. SUPPLEMENTARY NOTES

12a. DISTRIBUTION/AVAILABILITY STATEMENT

Approved for Public Release; Distribution Unlimited

12b. DISTRIBUTION CODE

13. ABSTRACT *(Maximum 200 words)*

Candidate substrate materials for the pseudomorphic growth Cu films as host templates on which to subsequently deposit diamond films have been selected. The selection criteria were (1) high diamond nucleation density as a bulk substrate; (2) low strain energy density in the interlayer material upon 100% two dimensional matching with the substrate; (3) ease of deposition of the interlayer material; and (4) low solubility at growth temperatures. The most promising interlayer materials were Ni, Si, Hf and Ti. Experimentally, the deposition of 5Å of Ti on Cu increased the diamond particle density relative to bare Cu by an order of magnitude. No appreciable diffusion to Ti into Cu occurred and only a thin carbide layer was necessary for diamond nucleation. Raman spectroscopy has been employed to analyze residual compressive stress in four diamond films. The line shape analysis indicated that the Raman band is mostly Lorentzian for all four samples and that the main broadening mechanism is via life-time shortening due to scattering from Si and N impurity concentrations. The line width increased linearly as a function of peak position, indicative of a correlation between the impurities and stress.

14. SUBJECT TERMS

pseudomorphic interlayers, copper substrates, diamond, heteroepitaxy, nucleation, growth, Raman spectroscopy, impurities, stress

15. NUMBER OF PAGES

25

16. PRICE CODE

17. SECURITY CLASSIFICATION OF REPORT	18. SECURITY CLASSIFICATION OF THIS PAGE	19. SECURITY CLASSIFICATION OF ABSTRACT	20. LIMITATION OF ABSTRACT
UNCLAS	UNCLAS	UNCLAS	SAR

Table of Contents

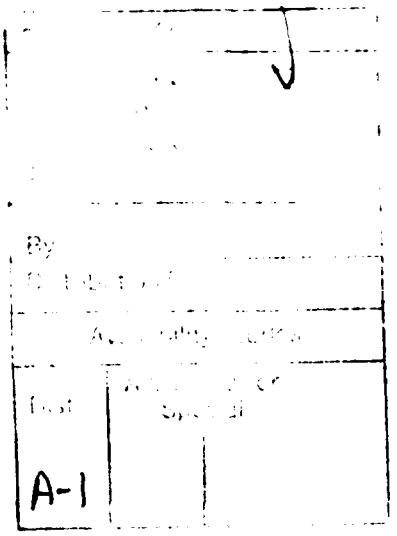

I. Introduction

Diamond as a semicon[illegible]in high-frequency, high-power transistors has unique advantages and disadvantages. Two advantages of diamond over other semiconductors used for these devices are its high thermal conductivity and high electric-field breakdown. The high thermal conductivity allows for higher power dissipation over similar devices made in Si or GaAs, and the higher electric field breakdown makes possible the production of substantially higher power, higher frequency devices than can be made with other commonly used semiconductors.

In general, the use of bulk crystals severely limits the potential semiconductor applications of diamond. Among several problems typical for this approach are the difficulty of doping the bulk crystals, device integration[illegible], high cost and low area of such substrates. In principal, these problems can be alleviated via the availability of chemically vapor deposited (CVD) diamond films. Recent studies have shown that CVD diamond films have thermally activated conductivity with activation energies similar to crystalline diamonds with comparable doping levels. Acceptor doping via the gas phase is also possible during activated CVD growth by the addition of diborane to the primary gas stream.

The recently developed activated CVD methods have made feasible the growth of polycrystalline diamond thin films on many non-diamond substrates and the growth of single crystal thin films on diamond substrates. More specifically, single crystal epitaxial films have been grown on the {100} faces of natural and high pressure/high temperature synthetic crystals. Crystallographic perfection of these homoepitaxial films is comparable to that of natural diamond crystals. However, routes to the achievement of rapid nucleation on foreign substrates and heteroepitaxy on one or more of these substrates has proven more difficult to achieve. This area of study has been a principal focus of the research of this contract.

At present, the feasibility of diamond electronics has been demonstrated with several simple experimental devices, while the development of a true diamond-based semiconductor materials technology has several barriers which a host of investigators are struggling to surmount. It is in this latter regime of investigation that the research described in this report has and continues to address.

In this reporting period, potential materials suitable both for pseudomorphic interlayers on Cu substrates and as templates for the deposition of diamond films have been selected and employed. The selection criteria revealed the most promising interlayer materials to be Ni, Si, Hf and Ti. The deposition of a very thin (≤5A) film of any one of these materials creates a strained interlayer of a material known to enhance the nucleation and growth of diamond films and which is now lattice matched to diamond as a result of its pseudomorphic growth on the Cu substrate. Experimentally, the deposition of 5Å of Ti on Cu increased the diamond particle density relative to bare Cu by an order of magnitude. No appreciable diffusion to Ti

into Cu occurred and only a thin carbide layer was necessary for diamond nucleation. Raman spectroscopy has been employed to analyze residual compressive stress in four diamond films. The line shape analysis indicated that the Raman band is mostly Lorentzian for all four samples and that the main broadening mechanism is via life-time shortening due to scattering from Si and N impurity concentrations. The line width increased linearly as a function of peak position, indicative of a correlation between the impurities and stress.

The following subsections detail the experimental procedures for each of the aforementioned studies, discuss the results and provide conclusions and references for these studies. Note that each major section is self-contained with its own figures, tables and references.

II. Use of Interlayers on Copper for Improved Diamond Heteroepitaxy

A. Introduction

Despite a significant amount of research on the CVD of diamond films, heteroepitaxial growth has been limited by the lack of close lattice-parameter matched substrates. The majority of substrates used for diamond growth have been refractory metals that form a carbide prior to the nucleation of diamond. These materials produce high particle densities; however, they have yet to show any epitaxial growth of diamond. Heteroepitaxial diamond crystallites have been produced on c-BN, Si, and Ni substrates [1-3], but monocrystalline films have not been produced. The success of c-BN and Ni substrates most likely came from the low lattice parameter mismatch (1.3% and 1.2%, respectively), while the success of Si, with a 34% lattice parameter mismatch, most likely came from the presence of an SiC interlayer.

This project involved a material selection process to help identify which materials would be suitable candidates for pseudomorphic deposition on copper. This will combine the high nucleation density of diamond property of the interlayer material with the close lattice-parameter match of copper. To investigate the integrity of titanium pseudomorphic layers in the diamond growth environment, thin layers were deposited on polycrystalline copper and the diamond particle density was correlated to the thickness.

B. Experimental Approach

Materials Selection. The material selection criteria for the interlayer materials consisted of four factors: 1) high diamond nucleation density as a bulk substrate; 2) low strain energy density in the interlayer material upon 100% two dimensional matching with the substrate; 3) ease of deposition of the interlayer material; and 4) low solubility at growth temperatures. The first step of the material selection process came from the work done by Wolter *et al.* on Si and various refractory materials.[4]

The second step of the selection process used a program called ORPHEUS developed by Braun.[5, 6] The program overlays the reciprocal surface nets of the substrate and overlayer candidate material. The user is then interactively aided to match the periodicity of the overlayer surface net and the substrate surface net. The change in the reciprocal lattice vector for the overlayer material is then used to calculate the strain energy density in the overlayer as well as the dislocation density. This computer model is relatively simplistic in that it only considers geometric factors, assumes the overlayer's elastic properties are the same as a bulk sample, and neglects other factors such as bond configurations, interdiffusion, and chemical reactions occurring between the substrate and the overlayer. Nevertheless, this program has successfully predicted the observed heteroepitaxial orientation between diamond/β-SiC and diamond /c-BN systems.[7, 8]

Deposition Description. Once the candidate materials had been evaluated for their "tendency to yield epitaxy," they were evaluated on the their ease of deposition on copper. The deposition technique was a resistive filament evaporation system connected *in-vacuo* to the diamond growth CVD chamber and a surface analysis chamber capable of performing Auger electron spectroscopy (AES), x-ray photoelectron spectroscopy (XPS), and low energy electron diffraction (LEED). The interlayer materials, with the exception of Si, were 2.0 mm rods inserted into copper leads and were heated using a Sorensen DCX 10-80B power supply. (Alternative methods for the deposition of silicon are being pursued.) The base pressure of the chamber was below 10^{-8} Torr and the deposition pressure was in the 10^{-8} Torr range. All substrates were polished down to 1μm diamond grit followed by final polishing using 0.3 μm and 0.05 μm alumina powders. An acid cleaning was performed to reduce the amount of oxygen on the surface and an H_2 plasma cleaning was performed to further remove any oxygen and carbon contaminants.

Growth of the diamond films used a MPCVD system and the bias-enhanced nucleation (BEN) technique. The biasing conditions were a voltage of -275 Vdc with a current of 45mA and a CH_4:H_2 ratio of 5% in a flow rate of 500sccm of H_2 for 10 minutes. The growth conditions were a CH_4:H_2 ratio of 0.2% in a flow rate of 500sccm of H_2 and a growth time of 5 hours. The substrate temperature was approximately 550°C during the BEN step and 600–700°C during growth.

C. Results and Discussion

Materials selection results. Based upon the results by Wolter *et al.*[4] of nucleation density of diamond on a variety of substrates using the BEN technique, Si, Ti, and Hf were chosen as potential interlayer materials. The nucleation densities found in that work are shown in Table I. Although not included in the work by Wolter *et al.*, Ni has shown promising potential as a substrate capable of producing heteroepitaxial diamond growth[1] and for that reason Ni was considered in subsequent stages of the selection process.

Table I. Nucleation of diamond on various refractory substrates after 60 minutes of biasing at -250V.[4]

Substrate	Particle density (cm^{-2})
Si	3×10^{10}
Ti	5×10^{9}
Ta	7×10^{7}
Hf	7×10^{9}

The second stage of the selection process was the two-dimensional matching of the substrate and the candidate interlayer material through the use of the ORPHEUS program. Those results are summarized in Table II. The strain energy density was lowest for Hf{0001} interlayers on Cu{111} surfaces with the next lowest being Ni{001} interlayers on Cu{001} surfaces. The carbides of the candidate material, where reliable data could be found[9], was also included because part of the growth sequence is the formation of a carbide layer prior to diamond formation. The best two candidate systems from this stage of the selection process were Ni(001) on Cu(001) and Ti(0001) on Cu(111).

Table II. Interfacial 2-D matching of Cu substrate and candidate interlayer materials. Diamond is added as a reference.

Interlayer Material	Parallel Planes		Strains			Strain Energy Density ($\times 10^{11}$ erg cm^{-3})	Misfit Dislocation Spacing (NND)
	Cu	Interlayer	ε_{xx} %	ε_{yy} %	γ_{xy} %		
Diamond	{001}	{001}	1.2	1.2	0	0.0019	79.6
Ni	{001}	{001}	2.4	2.4	0	0.013	30.1
Ti	{100}	{0001}	25.6	2.6	40	1.16	2.7
TiC	{001}	{001}	16.3	16.3	0	1.12	4.7
Ti	{111}	{0001}	9.6	9.6	0	0.14	18.3
TiC	{111}	{111}	16.3	16.3	0	1.2	6.8
Si	{001}	{001}	33.5	33.5	0	2.0	1.7
SiC	{001}	{001}	17.2	17.2	0	1.1	3.9
Ta	{001}	{001}	9.2	9.2	0	0.19	8.4
TaC	{001}	{001}	19.0	19.0	0	2.0	3.9
Hf	{111}	{0001}	1.1	1.1	0	0.00247	110.0

The third step in the selection process was ease of deposition for the resistive filament evaporation system. The primary concern for this step was the melting temperature of the material to be evaporated. A lower melting temperature was preferred because less power will be required to deposit the material and the lifetime of the evaporation source will be extended. Based on this criteria, nickel and titanium were the most promising material, while tantalum was the least preferred and dropped from subsequent consideration. Listed in Table III are the melting temperatures of the materials under consideration.

The fourth step was to consider the degree of solubility of the candidate material in Cu at typical growth temperatures. Listed in Table IV is the maximum solubility of the materials in Cu and the temperature at which maximum solubility occurs. Examination of Table IV indicates that solid solution formation is possible for all the materials especially when one remembers that only small amounts of the material will be used to form the interlayer.

Table III. Table of melting temperatures of candidate interlayer materials.[10]

Interlayer Material	Melting temperature (°C)
Hf	2231
Ni	1455
Si	1414
Ta	3020
Ti	1670

Table IV. Table of solubility of candidate materials in Cu and temperature of maximum solubility.[11]

Element	Weight percent solubility in Cu (wt%)	Temperature of maximum solubility (°C)
Ni	100	>354.5
Si	0	—
Ti	2.1	790
Hf	0.3	1295

The final consideration (Table IV) revealed that Ni will almost instantaneously form a solid solution for reasonable growth temperatures. This criteria revealed the need to find a method(s) to kinetically limit the formation of a solid solution or alloys between the copper and the interlayer material. One method will be to carburize the interlayer quickly to limit interdiffusion. Because Ni does not form a stable carbide, another method is needed. Yang *et al.*[1] showed that the formation of a hydride of Ni was the technique needed to form epitaxial diamond and a method similar to theirs will be used in this work. As a result of the material selection process, Ti was chosen as the first material to be used as an interlayer because of its ease of deposition.

Deposition Results. The thickness of the titanium overlayer was determined by x-ray photoelectron spectroscopy (XPS). A time series of titanium deposition on copper and XPS analysis provided a time dependent decay of the Cu $2p_{3/2}$ peak. This is illustrated in Fig. 1 and is consistent with layer-by-layer growth.[12] Once a layer-by-layer growth mode had been established, a deposition rate could be determined from a simple electron decay equation.

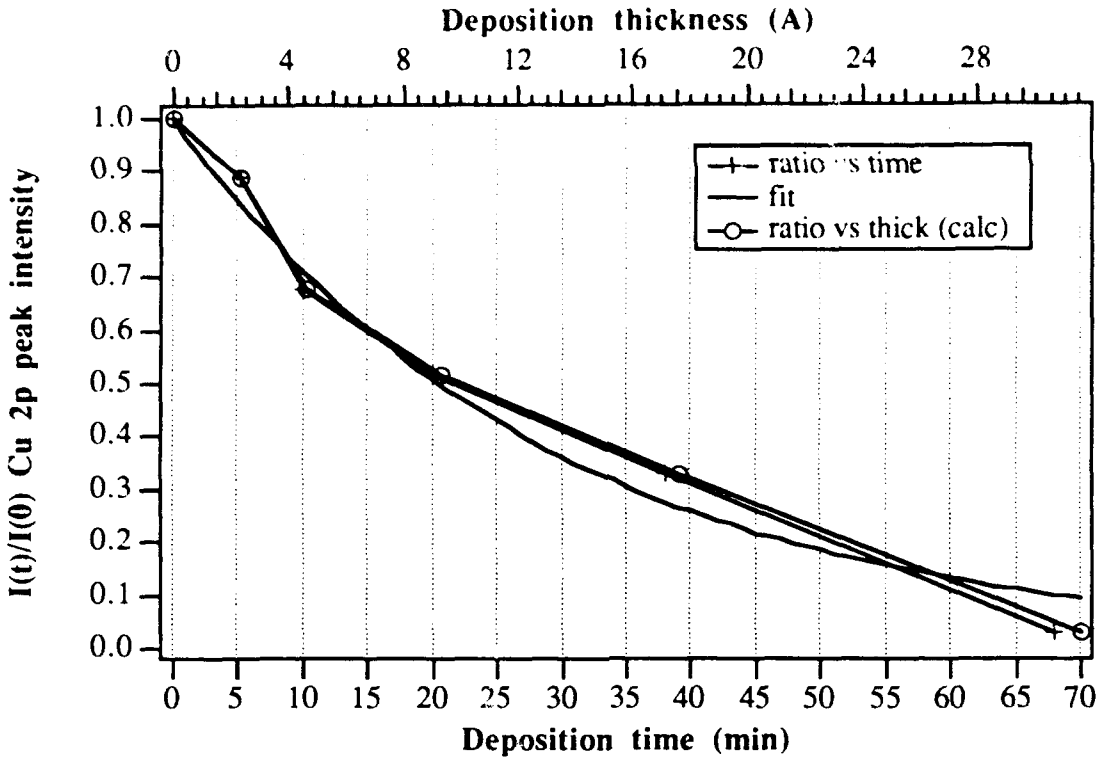

Figure 1. Peak intensity of the Cu $2p_{3/2}$ photoelectron peak as a function of deposition time. The deposition thickness was determined by a layer-by-layer exponential decay of the photoelectrons.

The resulting diamond particle densities after bias-enhanced nucleation and growth are displayed in Figure 2 and bulk copper and titanium are provided for comparison. The particle density for the bare copper after the biasing pretreatment was approximately 4×10^7 cm^{-2} and the particle density on the bulk piece of titanium (0.80 mm thick) was approximately 2×10^{10} cm^{-2}. Deposition of 5Å of titanium dramatically increased the particle density to 7×10^9 cm^{-2}. The relevance of this result is two-fold: 1) titanium remains on the surface for diamond nucleation to take place, and 2) only a thin carbide layer is necessary for diamond nucleation to take place.

D. Conclusions

The material selection process revealed that Ni, Si, Hf and Ti are the four most promising materials based on their high nucleation densities as a bulk material, ease of deposition as a thin film, and "tendency to yield epitaxy" on a Cu substrate. In addition, Ni and Si have demonstrated the ability to produce heteroepitaxial diamond crystals under the proper conditions. For the initial experiments, the XPS surface analysis technique has been used to determine the thickness of titanium on polycrystalline copper and the BEN technique has been used to increase the diamond particle density by more than one order of magnitude compared to bare copper.

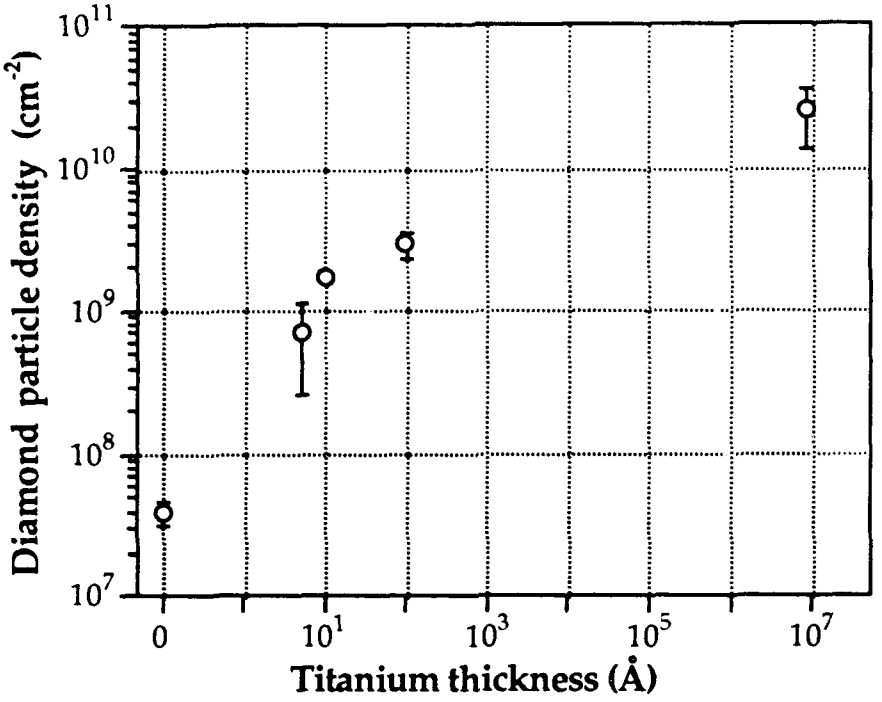

Figure 2. Plot of diamond particle density versus titanium overlayer thickness on copper after 10 min. of bias enhanced nucleation and 5 hours growth.

E. Future Research Plans and Goals

The future direction of this research plan is to investigate the remaining three candidate materials and determine optimum conditions for bias-enhanced nucleation of diamond. The best candidate material will than be investigated on single crystal copper substrates.

F. References

1. P. C. Yang, W. Zhu and J. T. Glass, J. of Material Research, **8**(8), 1773-1776 (1993).
2. B. R. Stoner, Doctor of Philosophy thesis, North Carolina State University, 1992.
3. S. Koizumi, T. Murakami, T. Inuzuka and K. Suzuki, Applied Physics Letters, **57**(6), 563 (1990).
4. S. Wolter and J. T. Glass in *Proceedings of The Electrochemical Society Spring Meeting at Honolulu, Hawaii*, (Electrochemical Society, Pennington, NJ, in press).
5. M. W. H. Braun, D. Sc. Thesis, University of Pretoria, South Africa, 1987.
6. M. W. H. Braun and J. H. van der Merwe, S. African J. Sci., **84**, 670 (1988).
7. M. W. Braun, H. S. Kong, J. T. Glass and R. F. Davis, **69**, 2679 (1991).
8. W. Zhu, X. H. Wang, B. R. Stoner, G. H. M. Ma, H. S. Kong, M. W. H. Braun and J. T. Glass, Physical Review B, **47**(11), 6529-6542 (1993).
9. G. Simmons and H. Wang, *Single Crystal Elastic Constants and Calculated Aggregate Values: A Handbook*, (M.I.T. Press, Cambridge, MA, 1971).
10. *CRC Handbook of Chemistry and Physics*, 73 edn. (CRC Press, Boca Raton, FL, 1992).
11. *Alloy Phase Diagrams*, (ASM International, Materials Park, OH, 1992).
12. L. C. Feldman and J. W. Mayer, *Fundamentals of Surface and Thin Film Analysis*, (Elsevier, New York, 1986).

III. Raman Analysis of Stress in Diamond Films

A. Introduction

Knowledge about the internal stress in diamond films is critical to advances in film quality; the stress may interfere and degrade the mechanical, as well as the transport and optical properties of the films. Raman spectroscopy has proven to be a useful and non-destructive technique for evaluating the stress of diamond films. Analysis of the Raman line shape has also been proven to be a very useful tool in the prediction of the internal stress that exists in diamond films. In our research, we extend these techniques to the analysis of stress in diamond films with different impurity concentrations arising from different growth conditions, and show that the impurities play a very important role as sources of the stress.

In Section I, we present ar nalysis of the stress in four diamond films which were grown in different growth conditions and which contained different impurity concentrations. The evaluation of the net stress in these diamonds was inferred from the diamond Raman line shift positions. It has previously been found that the Raman frequency shifts linearly with the stress. A simple way to explain the dependence of the Raman peak position on stress may be obtained by considering the relation $\nu_0 \alpha (k/m)^{1/2}$. In this relation ν_0 is the Raman peak frequency, k is the spring constant and m is the atomic mass. Upon applying compressive stress the atomic distance in the crystal is shortened. This change in distance manifests itself in a bigger spring constant k, and consequently a shift to a higher Raman frequency takes place: the larger the stress, the higher the Raman frequency shift. If the stress is tensile than the Raman shift is toward a lower Raman frequency. From the Raman line frequency shift, information about the stress type (compressive / tensile) and stress magnitude may thus be obtained using the above method.

The Raman line shape and line width (FWHM) on the other hand may convey information about the physical identity of the stress sources. The width of the Raman line is usually due to two main mechanisms referred to as the homogeneous and the inhomogeneous broadening. The homogeneous broadening is due to the life-time shortening of the crystal phonons. The theory of spectral line shape predicts that the line width is inversely proportional to the phonon life-time and that the line shape can be described by a Lorentzian function: $I(\nu)=I_0/\{1+((\nu_0-\nu)/(0.5*w))\text{^}2\}$ where I_0 is the maximum intensity, ν_0 is the central Raman frequency and w is the line width. In a very impure material, like our diamond films, the impurities and the grain boundaries are likely to be the principal sources of the shortening of the phonon life-time since they act as obstacles to the phonon propagation.

The inhomogeneous line broadening is due to a distribution of the central Raman frequency ν_0 which arises from inhomogeneities in the crystal environment. When the inhomogeneous mechanism is dominant, the line is expected to be of a Gaussian shape:

$I=I_0*\exp\{-((\nu_0-\nu)*1.6651/w)^2\}$. It has been proposed that one plausible cause of the inhomogeneous component in the diamond film Raman line may be the difference in the impurity distribution in each of the grains [1]. Hence each grain contributes a Raman band (homogeneous) with its characteristic ν_0 (which depends on the impurity distribution) and the resulting line shape is the envelop line over all the Raman bands contributed from all the grains. Schematic representations of a pure homogeneous and inhomogeneous mechanism are given in Figs. Ia and Ib.

Our Raman analysis of the peak positions indicates that each of our diamonds exhibits a net compressive stress. The net compressive stress found in each of the diamonds may be expressed as the algebraic sum of its compressive (-) and tensile (+) stress components. In this work we deconvoluted the observed net compressive stress into its compressive and tensile components and evaluated their magnitudes. Our work was based on models given in the literature for applicable stress sources in diamond films such as the thermal stress and the stress imposed by grain boundaries. After compensating for these stresses, we found that the diamond films still exhibited residual compressive stress. The line shape analysis indicated that the Raman band is mostly Lorentzian for all the four samples and that the main broadening mechanism is via life-time shortening due to impurity scattering. Moreover, the line width was found to be a linearly increasing function of the peak positions, indicative of a correlation between the impurities and the stress. Hence, we suggest the conclusion that the residual compressive stress component in our thin diamond films is mainly due to the various impurities in these samples.

Four diamond samples were deposited on silicon substrates using three different growth methods. One sample was grown using enclosed combustion chamber and will be referred to as the combustion sample. Another sample was grown using MWCVD and will be referred to as the 20h sample. The other two samples were deposited by hot filament method and are referred as the HF0%n and HF0.2%n which reflects their nitrogen composition.

B. Stress Calculation

In this section we present an analysis of the stress in the diamond samples as predicted from the Raman line shift. The key idea of our approach is to analyze internal stress in our diamond films building on results previously obtained which relate Raman line shift in single crystal diamonds to external compressive stress. Fig. 2 shows the diamond and the graphitic Raman signals for the four samples. Figure 3 shows the high resolution normalized Raman spectra of the diamond signal of these samples. The data for this experiment was obtained utilizing Micro-Raman spectroscopy at room temperature. In Table I a summary is given of the analyses obtained from Figs. 1 and 2.

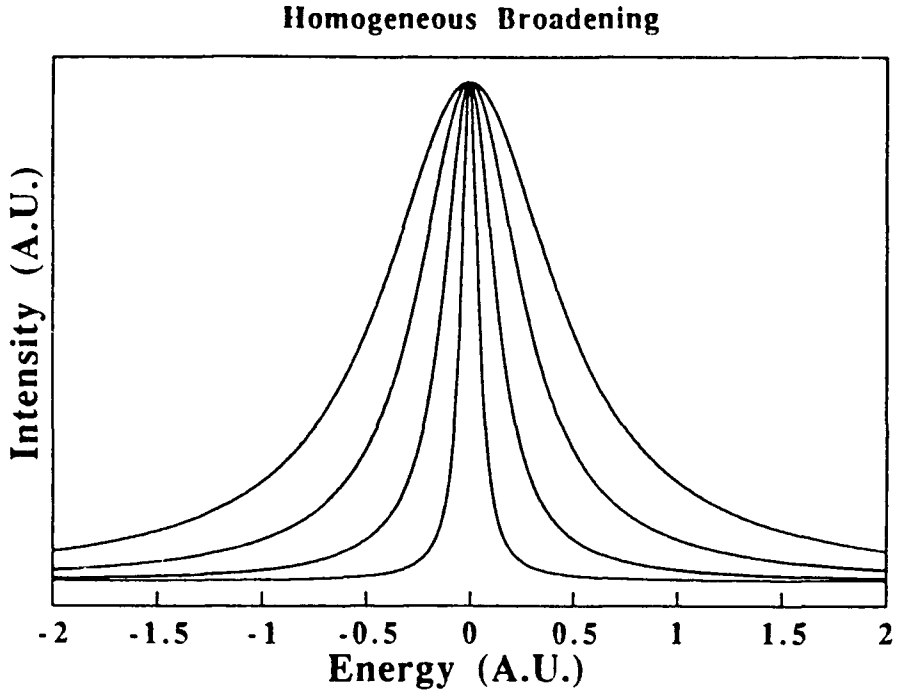

Figure 1a. Homogeneous broadening.

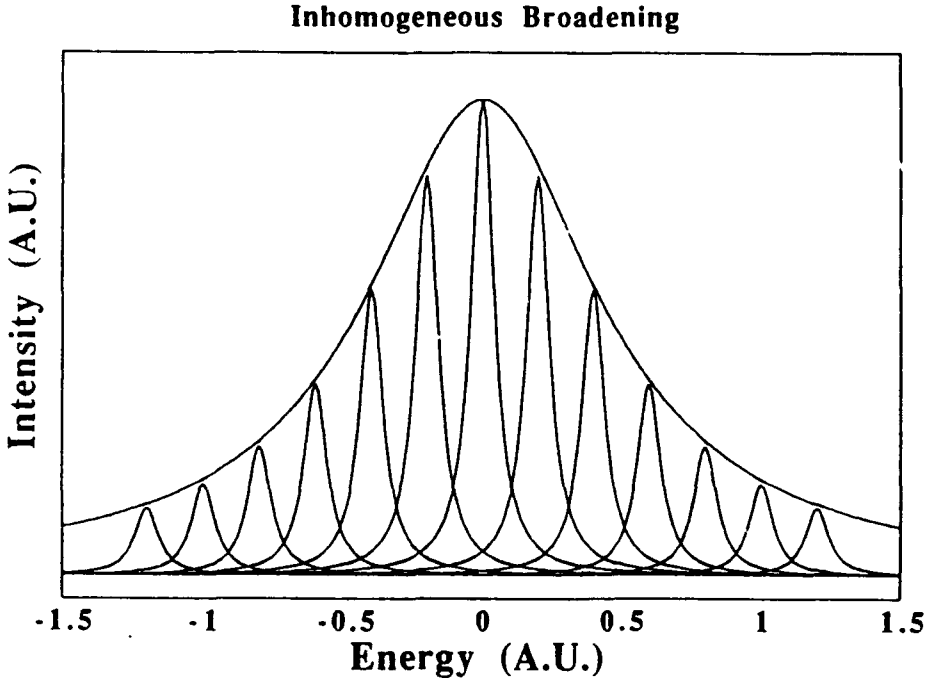

Figure 1b. Inhomogeneous broadening.

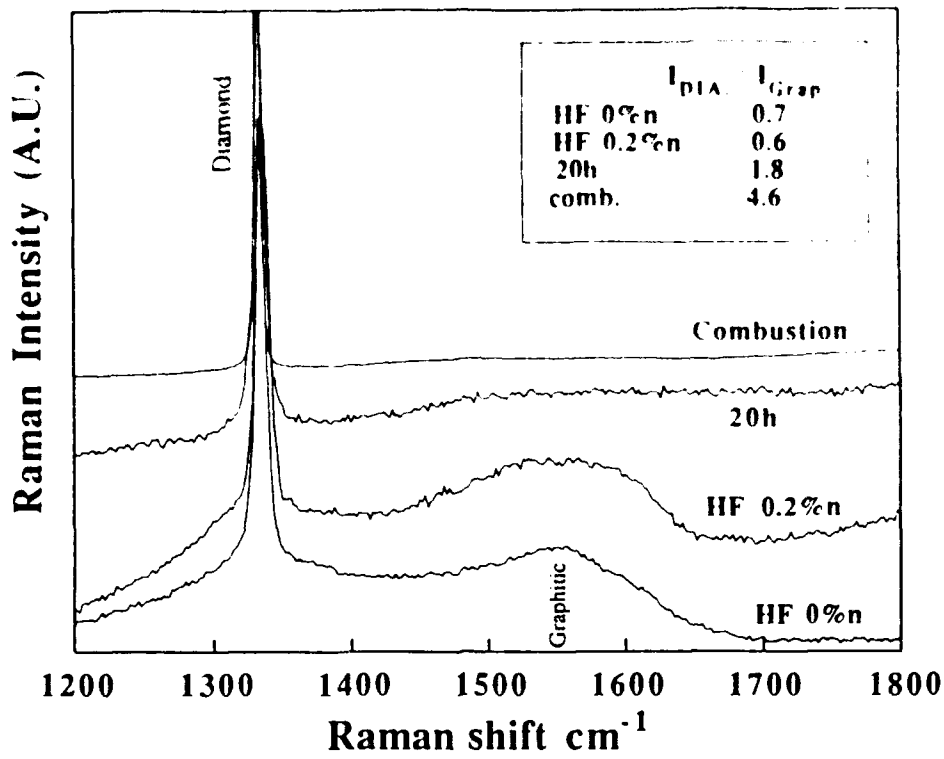

Figure 2. Diamond and graphitic Raman signals for the four samples.

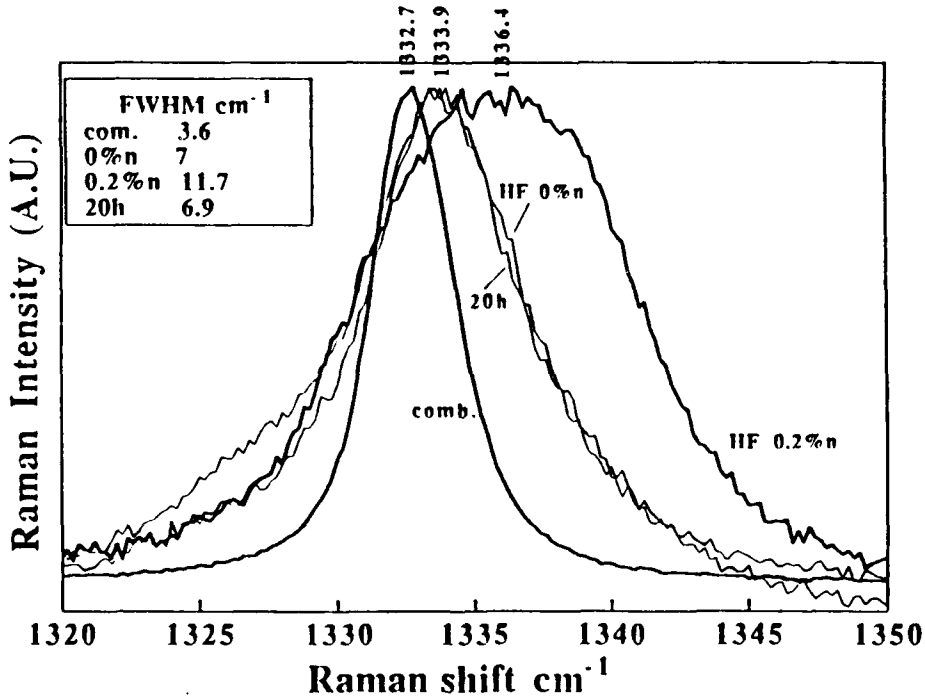

Figure 3. High resolution normalized Raman spectra of the diamond signal of these samples.

Table I Summary of Analyses

sample	growth T [C°]	FWHM [cm^{-1}]	Diamond peak position [cm^{-1}]	I_{DIA} I_{GRAPH}
combustion	1000	3.6	1332.7	4.6
20h	750	6.9	1333.9	1.8
HF 0%n	850	7	1333.9	0.7
HF 0.2%n	850	11.7	1336.4	0.6

The peak position ν_0 of natural and synthetic diamond crystals at room temperature has been reported to be in the range of 1332.1–1332.6 cm-1 with a full width at half maximum (FWHM) in the order of 1.8 cm-1. Upon applying external compressive stress (pressure) on the diamond, the peak position of the Raman signal was found to shift linearly with the stress to a higher frequency. The dependence of the Raman shift $\Delta\nu$ on the applied stress σ is

$$\Delta\nu=\nu-\nu_0=-\alpha\sigma \quad (1)$$

were ν_0 is taken to be the Raman peak position of the natural diamond when no pressure is applied and α is the pressure coefficient. The pressure coefficient depends on the nature of the applied stress and on the crystallographic direction of the diamond. Table II lists values of α's that have been found experimentally for uniaxial and hydrostatic stresses.

Table II. Values of α's Found Experimentally for Uniaxial and Hydrostatic Stresses

Stress	α [cm^{-1} / GP]
uniaxial compressive	2.37
hydrostatic	2.96
hydrostatic	2.87
hydrostatic	3.2

The effect of the uniaxial compressive stress, along the (001) and (111) directions, on the Raman line shift has also been previously measured. It was there found that the (001) face of the crystalline diamond has the lowest yield under pressure with α (001)=0.7 cm^{-1}/GP, while the (111) face reacts to the pressure with α(111)=2.2 cm^{-1}/GP, which is comparable to the values listed in Table II.

We can now use Eq. 1 to conversely infer the stress in the our diamond films from the observed Raman line shift. It must be noted, however, that depending on the direction of the Raman shift the predicted net stress could be either tensile (positive) or compressive (negative). From the observation that all our Raman lines shifted to higher energies, it may be concluded that all the diamond samples involved in this work exhibit a net compressive stress. In order to estimate the magnitude of the compressive stress in our diamond films, it is first imperative to choose the proper α. One approach is to average the α values; however, one must carefully determine how much weight should be given to α (001) since its value is the lowest. From the X-ray analyses we performed, presented in Table III, and from the SEM micrographs it may be concluded that the (100) diamond faces, in the samples, are missing or are in relatively small percentage. Therefore, we may conclude that the (100) is not a preferred orientation in the diamond grains. Hence an average value α=2.4 cm^{-1}/GP has been used in the pressure calculations.

Table III. X-ray Analyses

plane	powder	HF 0%n	HF 0.2%n	20h	combustion
(111)	100	100	100	100	100
(220)	25	29	23	19	12
(311)	16	-	14	6	4
(400)=(100)	8	-	-	4	1.7
(331)	16	-	-	-	5.1

In order to estimate the experimental stress in the diamond samples, $\sigma_{net,exp}$, Eq. 1 is used with ν_0=1332.4 cm^{-1}. The results of the calculations are listed in Table IV.

Table IV. Results of Calculations

Film	$\Delta\nu$ [cm^{-1}]	$\sigma_{net,exp.}$ [GP]
combustion	0.3	-0.13
20h	1.5	-0.63
HF 0%n	1.5	-0.63
HF 0.2%n	4	-1.67

The above calculations clearly indicate that all the diamond samples involved in this work exhibit a net compressive stress. No net tensile stress was observed. Furthermore, the combustion film was found to exhibit the lowest compressive stress while the HF 0.2%n exhibited the highest value of the compressive stress.

C. Sources of Stress in Diamond Films

In this section we analyze the sources of stress in the diamond films by identifying the stress components and estimating their contribution to the net stress $\sigma_{net,exp}$ in each of the diamond samples. These contributions to the net stress may be either tensile (positive) or compressive (negative). In general, the observable net stress σ_{net} in the diamond films is given by Equation 2 in terms of the thermal stress σ_{TH}, the stress due to silicon-diamond lattice mismatch σ_{lm} and the intrinsic stress σ_{IN} :

$$\sigma_{net}=\sigma_{TH}+\sigma_{lm}+\sigma_{IN} \qquad (2)$$

The thermal stress, σ_{TH}, arises from the difference in the thermal expansion coefficients of silicon and diamond. As a result of this difference, the silicon substrate contracts more than the diamond film upon cooling from the elevated growth temperature down to room temperature. Hence the silicon substrate applies compressive stress on the diamond film. The dependence of the thermal stress on the deposition temperature has been previously calculated [2]. There it was found that the compressive thermal stress decreases, almost linearly, with increasing deposition temperature. Using their analysis, we anticipate that the 20h sample (750 C°) should have a compressive thermal stress component ~ 0.25 GP, the two HF samples (850 C°) should exhibit a lower stress ~ 0.23 GP and the combustion sample (1000 C°) should be under the lowest thermal stress ~ 0.2 GP.

It is important to note that in the thermal stress calculation described in [2], only the thermal coefficients of the silicon substrate and the pure diamond were considered without taking into account the contribution from the graphitic phase present in the diamond film. The graphitic component probably would act as to lower somewhat the thermal stress by an amount which would depend on its quantity in a given sample.

The stress in the diamond due to its lattice mismatch with the silicon substrate (or with the SiC buffer layer) is expected to be tensile and to cause a very large Raman shift ~ 100 cm^{-1}. However, this order of magnitude was never observed in our diamond Raman lines. The absence of this stress can be attributed mainly to the dislocation relaxation mechanism. The presence of interfacial dislocations, in similar diamond films, has been confirmed previously. Hence we suggest that the lattice mismatch stress is not a contributor to the net stress in our diamond samples.

The intrinsic stress component, σ_{IN}, in the diamond film may be due to various sources such as impurities, structural defects such as dislocation, and interactions across grain boundaries. The main impurities in our samples are the presence of silicon and nitrogen, and the graphitic bonding. The nitrogen impurity is known to induce compressive stress in the diamond lattice while line structural defects such as dislocations may induce compressive or tensile stresses (depending on the sign of the Burger vector). The nature of the stresses due to the graphitic phase and the silicon center is still undetermined. The interactions across grain boundaries has been reported to be the possible origin of the main intrinsic tensile stress, $\sigma_{IN,GB}$, in the diamond films. In the next sections this tensile stress is quantified and an analysis is presented.

The interactions across grain boundaries is due to atomic attractive forces acting across both grain boundaries and voids, resulting in an induced tensile stress in the film. According to the model developed by Doljack et al. [3], the grains during growth are constrained by the substrate from lateral expansion. When the grains coalesce they exert attractive forces across the boundaries as a means of relaxing from the substrate constraint. The intrinsic tensile stress, $\sigma_{IN,GB}$, has been found to be inversely proportional to the average grain diameter, d, in a sample:

$$\sigma_{IN,GB}=[E(1-\nu)](\delta/d) \qquad (3)$$

were δ=0.077 nm is the constrained relaxation lattice constant of diamond and E(1ν)=1345 GP is the mechanical constant of diamond [2]. The average grain size for the combustion, 20h, HF 0%n and HF 0.2%n sample, as estimated from the SEM micrographs, is ~ 3.5, 1, 1.5, and 2.5 μm respectively. The values of $\sigma_{IN,GB}$ as well as the values of the previous stress components found so far are listed in Table V.

Table V. Values of $\sigma_{IN,GB}$ and Values of the Previous Stress Components

Sample	$\sigma_{net,exp}$ [GP]	σ_{TH} [GP]	$\sigma_{IN,GB}$ [GP]	$\sigma_{calculated}$ $=\sigma_{TH}+\sigma_{IN,GB}$	Δ [GP] $=\sigma_{net,exp}-\sigma_{calculated}$
combustion	- 0.13	- 0.155	+ 0.03	- 0.125	- 0.005
20h	- 0.63	- 0.25	+ 0.104	- 0.146	- 0.484
HF 0%n	- 0.63	- 0.23	+ 0.07	- 0.16	- 0.470
HF 0.2%n	- 1.67	- 0.23	+ 0.042	- 0.188	- 1.482

From the results listed in Table V it may be concluded that after compensating for the thermal and the grain boundary stress contributions ($\sigma_{calculated}$), three of the samples (20h, HF 0%n, HF 0.2%n) still exhibit an appreciable excess of compressive stress, which we refer to as Delta (Δ). We suggest that the most probable origin of Delta are the various types of impurities and the dislocations present in the diamond films. The validation of this hypothesis will be the subject of the following section.

D. Impurities as Intrinsic Stress Sources

Validation of the hypothesis that the intrinsic stress is due to impurities and dislocations may be obtained from analyzing the correlation of the Raman line broadening to the Raman shift position. Figure 4 presents such correlation obtained from our samples. It can be seen in the figure that the Raman peak position is a linearly increasing function of the Raman broadening. The broadening of the Raman line (FWHM) in diamond films is in general due to various mechanisms which may act simultaneously. One possible way to differentiate among them and determine their applicability to our case is by analyzing their correlation to the Raman shift position and line shape.

One possible mechanism which results in broadening is the Raman phonon confinement in a small domain size. The confinement model is based on the Uncertainty Principle which states: the smaller the domain size, the bigger the range of different phonons (with different q vector and different energy) that are allowed to participate in the Raman process. Hence the broadening of the Raman line in this case is due to the spread in phonon energy. According to this model, as the width of the Raman line gets broader, the peak of the line shifts to a lower energy. This behavior is opposite to our experimental results as indicated by the correlation presented in Fig. 4. A similar correlation to ours has been reported in [1]; their calculation led them to conclude that the broadening due to the confinement is not applicable when such a correlation is found. In light of the above we exclude the phonon confinement to be a principal cause of the Raman signal broadening in our type of diamonds.

A more plausible mechanism for Raman broadening in diamond films is the phonon scattering (phonon decay) at grain boundaries and at impurities. The scattering event shortens the lifetime of the phonons and thus results in a broader Raman line (as was discussed in the introduction to this chapter). The SEM micrographs of our samples indicate grain sizes of 1 μm or larger: this is a much larger dimension than the coherence length of the phonon (0.02 μm), hence the broadening due to grain boundaries is probably minimal. On the other hand, various type of impurities and dislocations, when in appreciable concentration, can act as an obstacle to the phonons and shorten their lifetime, thereby causing the broadening of the Raman line.

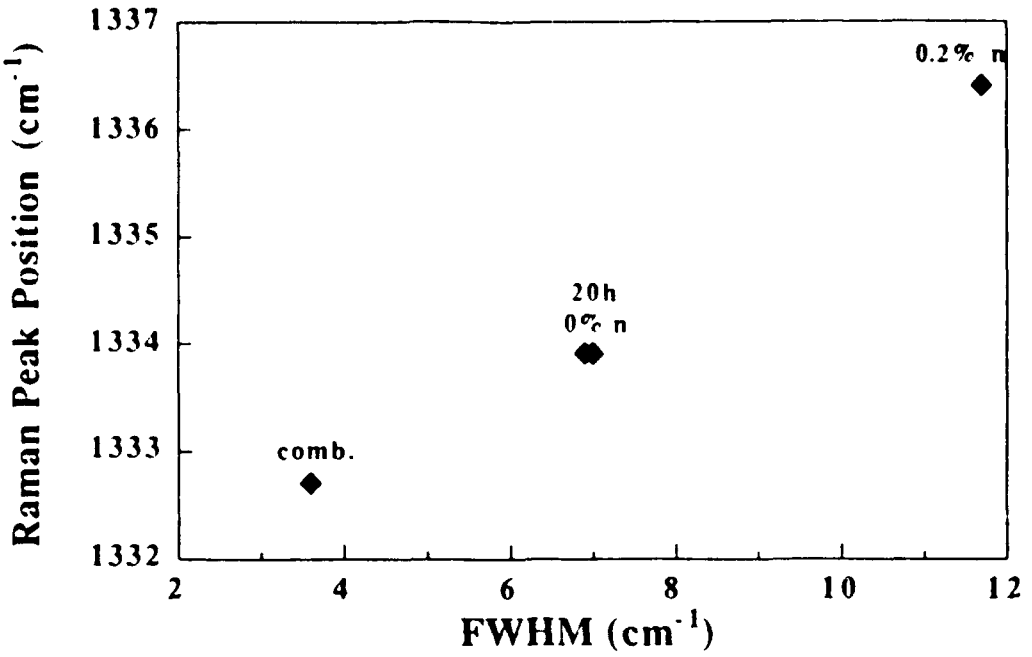

Figure 4.

To validate the applicability of the above mechanism in our case we first investigated the presence and type of various impurities in our samples. Identification of the types of impurities in the diamond films is obtained from the PL spectra presented in Fig. 5a and 5b. It can be seen that the spectra of the HF 0.2%n sample exhibits the nitrogen bands at 2.154 and at 1.945 eV and their vibronic side bands. The silicon center band at 1.681 eV is very weak. The spectra of the HF 0%n sample dose not show any of the nitrogen nor the silicon PL bands. The spectra of the 20h diamond sample is dominated by the strong silicon band while the spectra of the combustion diamond exhibits the nitrogen as well as the silicon PL bands. Another type of impurity which is present in these samples is the graphitic as can be seen from the Raman spectra in Fig. 2. The presence of dislocations was inferred from the line shape of the PL bands and will be discussed in detail in Chapter II. From the PL line shape we inferred that the HF 0.2%n sample possibly contains a very high concentration of dislocations and the combustion sample a relatively low concentration. No firm conclusions could be drawn from the PL line shape about the dislocation concentration of the 20h and the HF 0% samples; however, we speculate that it is moderate. (These two diamond films are not of as good a quality as the combustion diamond but neither so degraded as the HF 0.2%n.)

The Raman line broadening due to scattering at these impurities and dislocations is expected to be homogeneous (lifetime mechanism) and of a Lorentzian line shape. However, due to the probable differences of impurity distribution in each of the grains, a Gaussian component (inhomogeneous broadening) should be present as well. Figure 6 shows a line fit of a Lorentzian and a Gaussian function to the diamond Raman lines. It can be seen that all

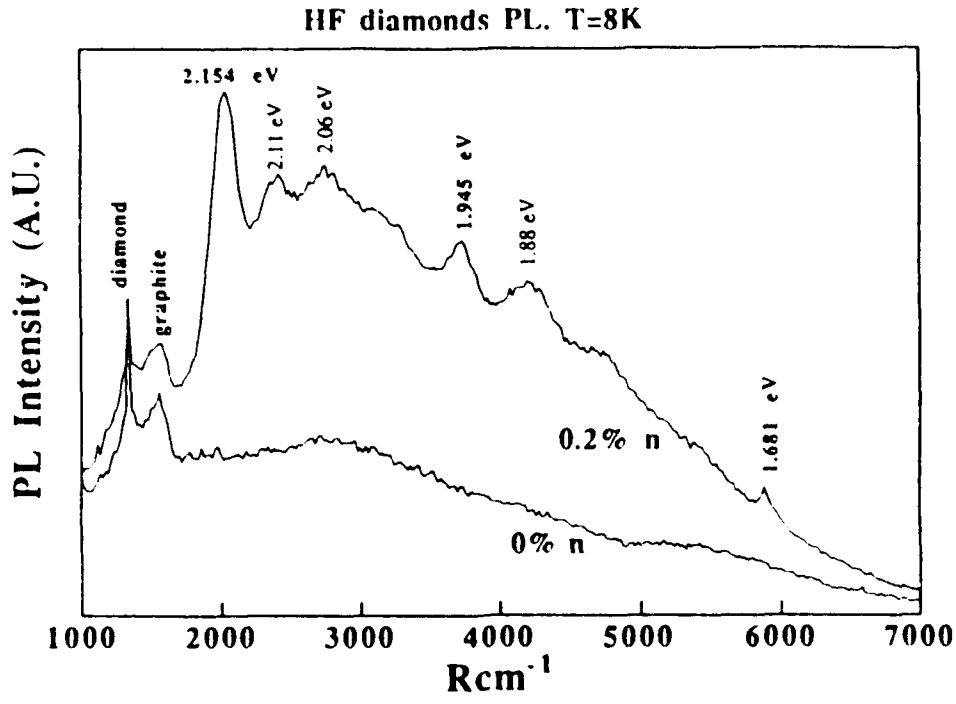

Figure 5a. HF diamonds PL. T=8K.

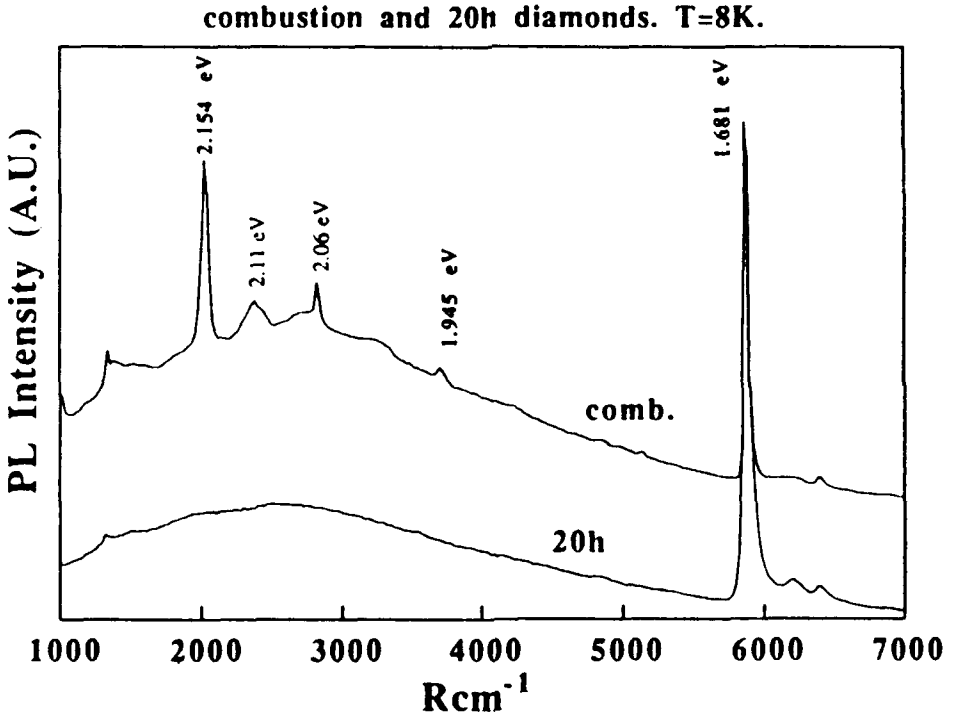

Figure 5b. Combustion and 20h diamonds. T=8k.

the Raman lines exhibit a more prominent Lorentzian component and less of a Gaussian component. Therefore, from our experimental observations we may conclude that the Raman broadening mechanism in our diamonds occurs via impurity scattering with a small contribution from the inhomogeneity in the impurity grain distribution. We note, however, that our analysis of the Raman line shape is a qualitative one due to the relatively weak Raman signal inherent to our type of thin diamond films which precludes numerical deconvolution of the Gaussian and Lorentzian components.

If the hypothesis that the impurities are the source of the internal stress is correct, then the width of the Raman lines can be expected to correlate well with the Raman peak positions, as was indeed found in our work (see Fig. 4). Our observed correlation between the Raman widths and the Raman peak positions indicates that the impurities, which were argued to cause the broadening, are also the main possible cause of the compressive internal stress in the diamond films. Hence we assign the origin of the excess compressive stress Delta (previously shown in Table V) to the various impurities and dislocations in the diamond film.

In the following section we investigate the contribution from each impurity to the stress Delta and relate the impurity concentration to the magnitude of the stress.

E. Contribution of Nitrogen, Silicon, Dislocations and Graphitic Bonding to the Stress

The graphitic phase has been suggested to be the principal impurity responsible for the internal stress in diamond films. To investigate the role of the graphitic phase as a source of internal stress in our films, we plotted its relative quantity $I_{graphitic}/I_{diamond}$ (obtained from the graphitic and diamond integrated areas of the Raman signals) versus the stress Delta. The graph is shown in Fig. 7, and for each sample also lists the other non-graphitic impurities found (and their relative quantities as will be discussed in the next paragraph). The weak correlation in Fig. 7 indicates that the graphitic phase cannot be the sole cause of the internal stress. The HF 0%n sample, for example, contains more than twice the graphitic phase than the 20h sample yet both samples exhibit the same internal stress. Hence the contribution to the stress from the other impurities present in each sample has to be taken into account as well.

In order to investigate the role of the silicon and nitrogen impurities and dislocations as sources of stress, it is imperative to obtain information about their concentration. However, finding the actual impurity concentration in our type of diamond is not a straightforward task. One advanced technique we used to measure concentration is the Secondary Ion Mass Spectroscopy (SIMS). Since this method can not differentiate between types of bonding there is no quantitative way to measure the graphitic concentration. Furthermore, under this method the assignment of absolute concentrations to the silicon impurities in the diamond

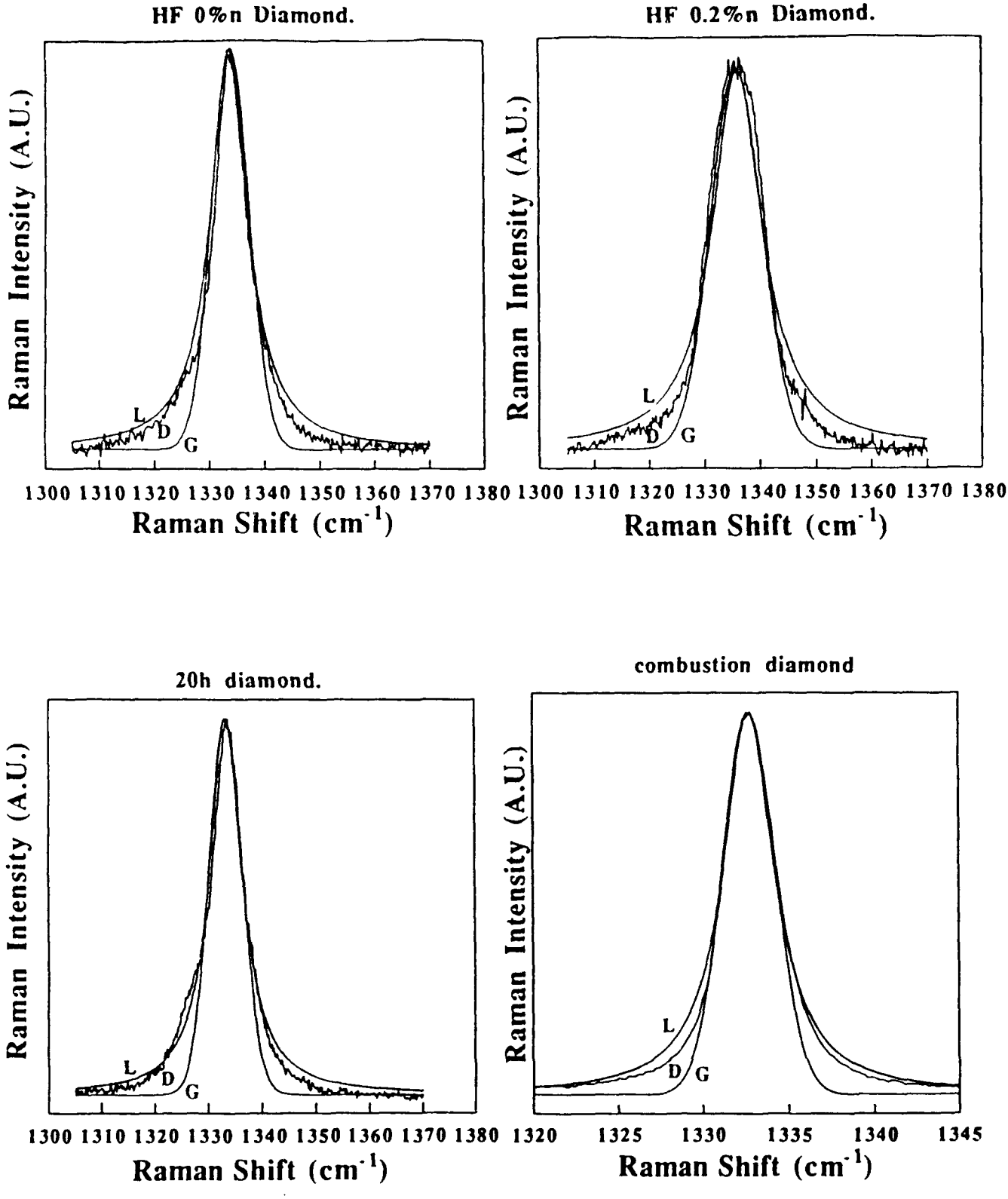

Figure 6. A line fit of a Lorentzian and a Gaussian function to the diamond Raman lines.

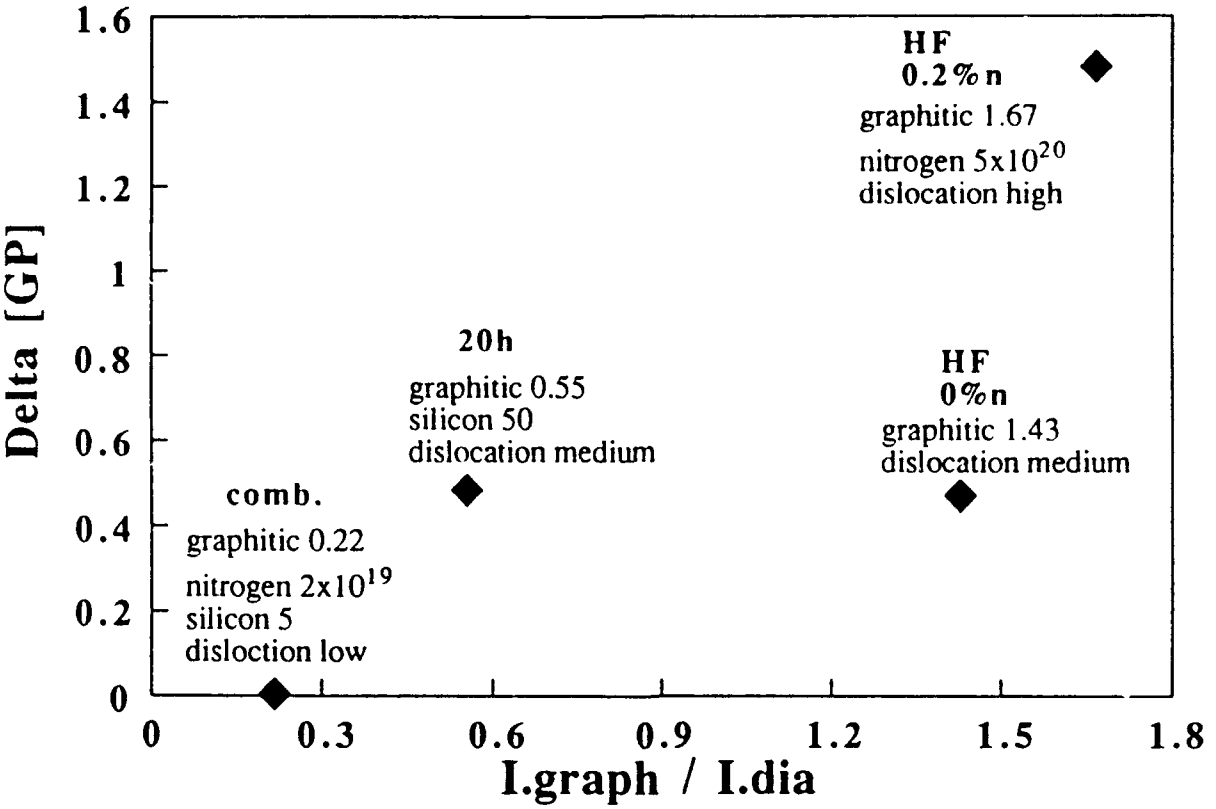

Figure 7. Relative quantity $I_{graphitic}/I_{diamond}$ of graphitic phase versus the stress Delta.

films was impractical due to the silicon substrate. The concentration of nitrogen impurities, on the other hand, was able to be measured but due to the grain morphology and partial coverage of our thin film diamonds, only an approximate value of the nitrogen impurity concentration could be obtained. Relative concentration of impurities may also be inferred from the integrated areas of the impurity PL bands and of the Raman signals. Table VI lists the relative quantity of each impurity in the samples and the method by which it was obtained.

From Table VI and Fig. 7 it be seen that the HF 0.2%n sample contains ~ 5×10^{20} nitrogen atoms/cm^3. This level of nitrogen concentration is very high and has been reported to be the upper limit that a type Ia diamond can contain. The HF 0.2%n also contains a relatively high amount of the graphitic phase and dislocations. Since the concentration of the graphitic phase in this sample is about the same as that in the HF 0%n sample, we attribute most of the compressive stress (~1 GP) in the HF 0.2%n sample to be due to dislocations and the very high nitrogen doping level. On the other hand, the HF 0%n sample contains more than twice as much of the graphitic phase than the 20h sample, yet both samples exhibit the same magnitude of stress. We suggest that the extra amount of stress in the 20h sample is due to the high concentration of silicon centers which are not present in the HF 0%n sample. The

Table VI. Relative Quantity of Each Impurity

sample	$I_{graphitic}/I_{diamond}$ Raman integrated area	$I_{silicon}/I_{diamond}$ PL integrated area	nitrogen [cm^{-3}] SIMS	dislocation PL line shape [concentration]
combustion	0.22	5	2×10^{19}	lowest
20h	0.55	50	nominal	medium
HF 0%n	1.43	nominal	nominal	medium
HF 0.2%n	1.67	nominal	5×10^{20}	highest

combustion diamond sample contains ~2×10^{19} nitrogen/cm^3: this level of nitrogen has been considered to be very low in the Ia type diamonds. The combustion diamond also contains a low concentration of silicon and graphitic impurities. The concentrations of these impurities in the combustion diamond are probably not high enough to induce any appreciable stress in the sample.

We conclude that the dislocations and silicon, graphitic and nitrogen impurities act as sources of intrinsic compressive stress in our diamond films, and that the magnitude of the stress depends on the concentration of the specific impurity.

F. References

1. J. W. Ager, D. K. Veirs, and G. M. Rosenblatt, Phys. Rev. B **43**, 6491 (1991).
2. H. Windischmann, G. F. Epps, Y. Cong, and R. W. Collins, J. Appl. Phys. **69**, 2231 (1991).
3. F. A. Doljack and R. W. Hoffman, Thin Solid Films **12**, 71 (1972).

IV. Distribution List

Mr. Max Yoder
Office of Naval Research
Electronics Program–Code 314
Ballston Tower One
800 North Quincy Street
Arlington, VA 22217-5660

Office of Naval Research
Resident Representative
The Ohio State Univ. Research Center
1960 Kenny Road
Columbus, OH 43210-1063

Director
Naval Research Laboratory
Attention: Code 2627
Washington, DC 20314

Defense Technical Information Center
Building 5
Cameron Station
Alexandria, VA 22314

Dr. Robert J. Markunas
Research Triangle Institute
Post Office Box 12194
Research Triangle Park, NC 27709-2194

Dr. Ron Rudder
Research Triangle Institute
P. O. Box 12194
Research Triangle Park, NC 27709-2194

Dr. Howard K. Schmidt
SI Diamond Technology, Inc.
2345 North Boulevard
Houston, TX 77098

Prof. Karl Spear
Pennsylvania State University
201 Steidle
University Park, PA 16802

Dr. Michael W. Geis
Lincoln Laboratories
244 Wood Street
P. O. Box 73
Lexington, MA 02173

Prof. R. F. Davis
Materials Science and Engineering
Box 7907
North Carolina State University
Raleigh, NC 27695-7907

Prof. R. J. Nemanich
Department of Physics
Box 8202
North Carolina State University
Raleigh, NC 27695-8202

Prof. John C. Angus
Chemical Engineering
Case Western Reserve University
Cleveland, OH 44106

Prof. Andrzej Badzian
271 Materials Research Laboratory
The Pennslyvania State University
University Park, PA 16802

Dr. H. Liu
Emcore Corp.
35 Elizabeth Avenue
Somerset, NJ 08873

Prof. Karen Gleason
Chemical Engineering, Rm. 66-462
M. I. T.
Cambridge, MA 02134

Prof. Jerry Whitten
Chemistry
Box 8201
N. C. State University
Raleigh, NC 27695-8201

Dr. Ray Thomas
Research Triangle Institute
Box 12194
Research Triangle Park, NC 27709-2194

Dr. Allen R. Kirkpatrick
Epion Corp.
4R Alfred Circle
Bedford, MA 01730

Dr. Robert C. Linares
Linares Management Assoc., Inc.
P. O. Box 336
Sherborn, MA 01770

Dr. Martin Kordesch
Physics
Clippinger Research Laboratories
Ohio University
Athens, OH 45701-2979

Prof. Charter Stinespring
Chemical Engineering, Box 6101
West Virginia University
Morgantown, WV 26506

Prof. Robert Hauge
Chemistry
Rice University
Houston, TX 77251

Dr. John Margrave
HARC
4800 Research Forest Drive
The Woodlands, TX 77381

Dr. John Posthill
Research Triangle Institute
P. O. Box 12194
Research Triangle Park, NC 27709-2194

Dr. James Butler
NRL Code 6174
Washington, DC 20375

Dr. Andrew Freedman
Aerodyne Research, Inc.
45 Manning Road
Billerica, MA 01821

Prof. Michael Frenklach
Penn State University
202 Academic Projects Bldg.
University Park, PA 16802

Prof. Jeffrey T. Glass
Materials Science & Engr.
Box 7907
North Carolina State University
Raleigh, NC 27695-7907

Dr. Warren Pickett
Code 6604
Naval Research Laboratory
Washington, DC 20375-5345

Prof. Max Swanson
Physics
University of North Carolina
Chapel Hill, NC 27599-3255

Dr. James Zeidler
Code 7601
NRaD
San Diego, CA 92152